Materials Advances

ROYAL SOCIETY OF CHEMISTRY

PAPER

View Article Online
View Journal | View Issue

Check for updates

Cite this: *Mater. Adv.*, 2025, 6, 2231

A reusable BTO-based composite film for safe and convenient tooth whitening†

Sihan Wang,[ab] Yang Zhou,[ab] Yunan Zhang,[ab] Zhongyi Yan,[ab] Liping Chen[ab] and Ling Guo ‡*[ab]

Received 29th December 2024,
Accepted 22nd February 2025

DOI: 10.1039/d4ma01293c

rsc.li/materials-advances

Dental surface staining is the most common problem in oral health care. The current mainstream treatment is still bleaching with high concentrations of hydrogen peroxide, which will not only cause enamel damage and tooth sensitivity but may also lead to periodontal soft tissue stimulation. Here, we have prepared a barium titanate (BTO)-based composite film doped with graphite (C) particles, which can gently and continuously produce hydroxyl radicals ($^{\bullet}OH$) and superoxide anions ($^{\bullet}O_2^-$) through the piezoelectric catalysis and thermal catalysis induced by the oral chewing movement and temperature changes. This composite film can replace the reactive oxygen species produced by hydrogen peroxide, destroying the conjugated double bonds of the stained macromolecules, degrading the dye macromolecules into light compounds, and finally achieving tooth whitening, but without causing damage to tooth enamel and cells. In the future, this BTO-based composite film may become a promising strategy for oral health care.

Open Access Article. Published on 10 March 2025. Downloaded on 7/21/2025 10:40:31 PM.
This article is licensed under a Creative Commons Attribution-NonCommercial 3.0 Unported Licence.

Introduction

Staining of the tooth enamel surface mainly originates from the deposition of exogenous pigment, which greatly affects the self-image and confidence of people in modern society.[1] Sources of exogenous pigment mainly include dark food (chocolate, grapes, blueberries, mulberries, beet, pomegranate, *etc.*), drinks (red wine, coffee, tea, coke, *etc.*), medical health care products (oral gargle, oral iron, Chinese medicine, *etc.*), and oral bad habits (using tobacco, betel nut, *etc.*).[2] Tannins,[2] tar, and nicotine[3] are very likely to adhere to the tooth surface and are difficult to completely remove mechanically. In the past few decades, high concentrations of hydrogen peroxide have been the mainstream whitening agents, as they produce a high concentration of hydroxyl radicals ($\cdot OH$) during decomposition. It has been reported that high concentrations of hydrogen peroxide products may produce a series of complications during tooth whitening due to their high permeability, including severe enamel destruction,[4,5] tooth sensitivity,[6] oral soft tissue irritation, and cytotoxicity.[7] Although these complications can be alleviated by reducing the concentration of hydrogen peroxide, the tooth-whitening effect will also be significantly reduced. Therefore, there is an urgent need to develop a novel and promising alternative strategy that produces a kind of mild, stable, and sustainable reactive oxygen species.

Barium titanate ($BaTiO_3$, BTO) is a material with both piezoelectric catalytic properties and thermal catalytic properties.[8] Spontaneous polarization can occur when the BTO is within the temperature range of 5–120 °C. Because of its excellent piezoelectric performance after polarization, BTO can activate the piezoelectric effect through mechanical stress, and produce charge separation, thus leading to electrostatic action on the surface of the material, and then achieving the purpose of promoting the catalytic reaction. Not only that, but BTO exhibiting a ferroelectric performance is also a kind of typically important thermoelectric material, that is, when the temperature changes (5–120 °C), it can lead to charge separation inside the material, forming an electric field, and then achieve the purpose of promoting the catalytic reaction. Therefore, BTO can exchange charges with water and oxygen molecules through oscillation and temperature change in the solution environment to generate a hydroxyl radical ($^{\bullet}OH$) and a superoxide anion ($^{\bullet}O_2^-$), thus destroying the conjugate double bonds (the key structure of dye color and stability) of organic pigment molecules, realizing an oxidation reaction transforming dye macromolecules into light compounds (Fig. 1c).[9] In the existing research, BTO has made outstanding contributions to environmental pollutant degradation due to the above excellent performance.[10] Recently, experimental results by Chaobo Dai and Yang Wang have shown that a hydrogel embedded with BTO particles can significantly whiten teeth stained by habitual

[a] *Luzhou Key Laboratory of Oral & Maxillofacial Reconstruction and Regeneration, Luzhou, China. E-mail: glsmiling@swmu.edu.cn*
[b] *Institute of Stomatology, Southwest Medical University, Luzhou, China*

† Electronic supplementary information (ESI) available. See DOI: https://doi.org/10.1039/d4ma01293c

‡ Correspondence to: Department of Oral prosthodontics, The Affiliated Stomatological Hospital, Institute of Stomatology, Southwest Medical University, 2 Jiangyang South Road, Luzhou, Sichuan 646000, China.

© 2025 The Author(s). Published by the Royal Society of Chemistry

Open Access Article. Published on 10 March 2025. Downloaded on 7/21/2025 10:40:31 PM.
This article is licensed under a Creative Commons Attribution-NonCommercial 3.0 Unported Licence.

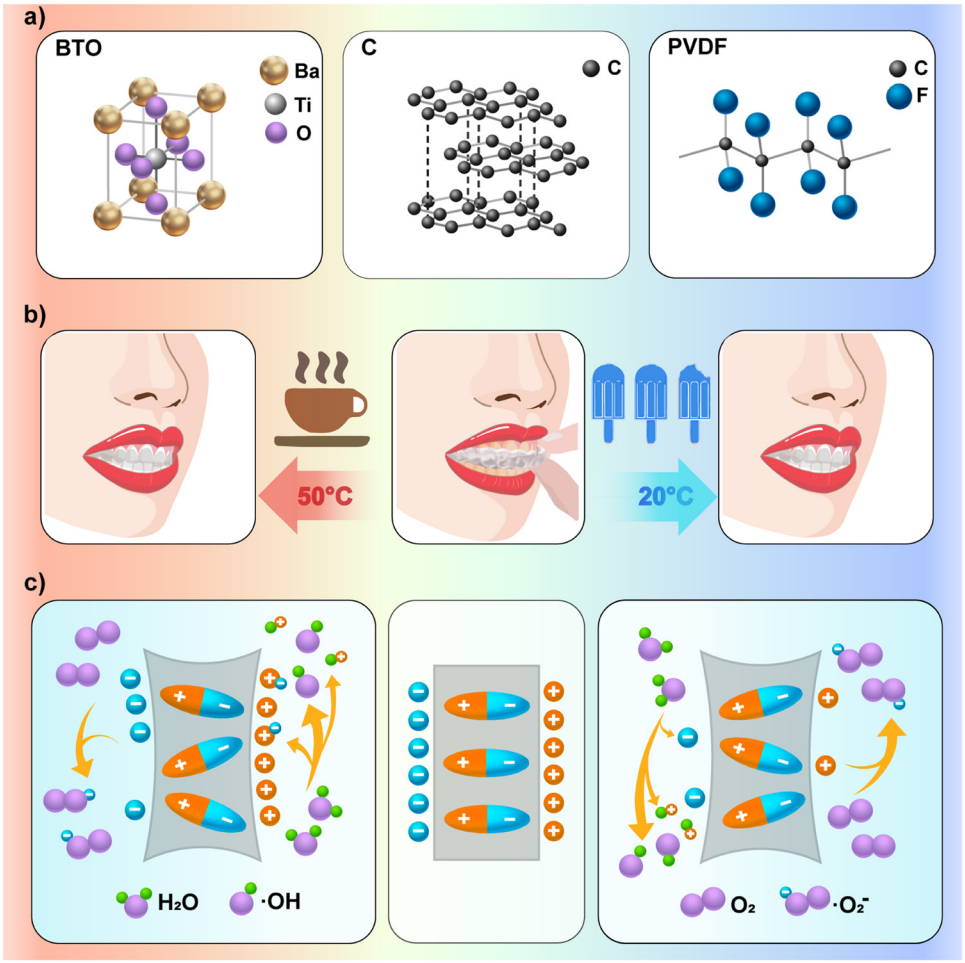

Fig. 1 Schematic illustration of the composition structure of the BCPCF and the working principle. (a) Schematic representations of the molecular structures of BTO, C and PVDF from left to right. (b) The BCPCF stimulated piezoelectric and thermal catalytic effects through mastication pressure and temperature changes. (c) BTO produced •OH and $•O_2^-$ *via* piezoelectric and thermal catalytic effects.

consumption of beverages and flavoring agents through daily oral temperature changes, respectively.[11,12] This may be an important signal that piezoelectric materials will be more used in the medical field of stomatology in the future.[13] However, due to the high mobility of hydrogel materials, these materials are mostly suitable for adding to toothpaste or whitening in the clinic.[14–16] This not only increases the economic cost of research and development and use, but also increases the inconvenience of patient use, and reduces the comfort of the tooth whitening process. Therefore, we want to develop an economical and efficient material—BTO-based composite film, which is convenient for patients to wear at any time without additional operation and can be used repeatedly.

Graphite (C) is a very easy-to-obtain and stable material, which does not easily react with other substances at room temperature. A large number of studies have shown that doped graphite can often play an important role in improving the piezoelectric materials' performance in terms of piezoelectric effect, pyroelectric effect, electrical conductivity, mechanical properties and wear resistance.[17–25] In addition, polyvinylidene fluoride (PVDF) is often used as a substrate to prepare a BTO composite film due to its flexibility and mechanical strength.[22,25–34] Using a solution casting method, the three components can be combined simply and effectively and worn on the teeth. The most common movements in the oral environment, such as speaking, chewing, eating, and drinking, subject the composite film to mechanical pressure and temperature changes in the mouth. And because the production of free radicals comes from the piezoelectric catalytic effect and the thermal catalytic effect, rather than the consumption of the material itself, the composite film can be used repeatedly. In this experiment, the BTO-based composite film (the BTO/C/PVDF composite film, BCPCF) we prepared did not cause enamel surface damage to the teeth and cytotoxicity. In this experiment, this tooth-whitening system based on piezoelectric catalysis and thermal catalysis showed important therapeutic feasibility.

Experimental

Materials preparation

Materials. Barium titanate ($BaTiO_3$, 99.9%, Ball type, D50 = 0.6–1 μm, Macklin), graphite (C, Analytical Reagent, Macklin), polyvinylidene fluoride (PVDF, Analytical Reagent, Shanghai

© 2025 The Author(s). Published by the Royal Society of Chemistry

Open Access Article. Published on 10 March 2025. Downloaded on 7/21/2025 10:40:31 PM. This article is licensed under a Creative Commons Attribution-NonCommercial 3.0 Unported Licence.

Sanaifu FR 904 powder), *N*,*N*-dimethylformamide (DMF, Analytical Reagent, 99.5%, Macklin), rhodamine 6G (RhB, Analytical Reagent, Macklin), 5,5-dimethyl-1-pyrrolic-*N*-oxide (DMPO, 98%, Crgent Biotech), dimethyl sulfoxide (GC, 99.8%, Macklin), human gingival fibroblasts (HGF, Procell), live/dead cell staining kit (Calcein AM, PI, UElandy), cell counting kit-8 (CCK-8, DOJINDO), DMEM high glucose medium (Gibco), Australian fetal bovine serum (HyClone), penicillin–streptomycin solution (Beyotime), trypsin (trypsin–EDTA digest (0.25%) containing phenol red, HyClone), serum-free cell freezing medium (Procell), phosphate buffer saline (pH 7.2–7.4, Solarbio), chloramine-T (Macklin), and hydrogen peroxide particles (Shunke Biological) were employed in this study.

Preparation of the BTO-based composite film (BCPCF). The PVDF powder was mixed with the *N*,*N*-dimethylformamide solution and magnetically stirred at a mass volume ratio of 1 : 9. After the PVDF was completely dissolved, the PVDF solution was obtained. Then, the BTO and graphite powder were added to the solution according to the PVDF : BTO : C ratio of 9 : 1 : 0.05, and further stirred until the BTO and graphite powder were evenly dispersed in the PVDF solution to obtain the BTO/C/PVDF mixed solution. Then the treated solution was placed on the glass plate and dried at the oven temperature (55 °C). After complete evaporation of *N* and *N*-dimethylformamide, the BTO-based composite film (BCPCF) was obtained.

Characterization of the BTO-based composite film (BCPCF). The microstructure of the composite film was characterized by field-emission scanning electron microscopy (SEM, ZEISS Merlin). A Fourier transform IR (FTIR) spectrometer and an X-ray diffraction system (XRD, Brooke D8) were used to observe the characteristic peaks and crystalline phase of each component.

Material performance testing of the BTO-based composite film (BCPCF)

The elastic material tensile test (Tt) consisted of two parts: The tensile measurement was tested per ISO527. During the test, the sample was clamped on the fixture of the tensile tester (Senstest, UTM4103), and then a gradually increasing tensile force was applied until the sample broke. The tensile force and the displacement data of the sample were recorded during the test, and the tensile strength σ of the sample was calculated according to formula (1). F represents the force, and A represents the cross-sectional area of the test material. The flexural measurement was performed by ISO178. The elasticity modulus E was calculated according to formula (2). σ represents stress and ε represents strain.

$$\sigma = \frac{F}{A} \tag{1}$$

$$E = \frac{\sigma}{\varepsilon} \tag{2}$$

A piezoelectric-responsive force microscope (PFM, MFP-3D) was used to detect local information changes in the surface piezoelectric properties of ferroelectric materials. By applying an AC voltage on the sample surface, the polarization direction of the sample surface and the electrical domain structure (the region in the material produced by the spontaneous polarization of the internal atoms or molecules, also called the electrical domain) were shown. When the external electric field was gradually increased, the electric domain in the crystal contrary to the external electric field was gradually reversed. The polarization strength of the crystal was enhanced. When the external electric field was weakened or it increased in the opposite direction, the crystal interior changed accordingly. The hysteresis circuit can be drawn based on the relationship between the ferroelectric material and the electric field.

Rhodamine 6G dye degradation test

5 mg L^{-1} rhodamine 6G (RhB) solution was diluted in a gradient of 2.5 mg L^{-1}, 1.25 mg L^{-1}, 0.625 mg L^{-1}, and 0.3125 mg L^{-1}. These solutions were tested at λ = 400 nm, 450 nm, 500 nm, 550 nm, and 600 nm in the microplate reader to draw the standard curve of RhB concentration and OD value.

Firstly, the mechanical pressure cycle test was conducted using the cold and heat cycle meter (TC-801F). The cold and hot water tanks were set to 37 °C, the slot conversion time was set to 20 s, and the tank residence time was set to 30 s. A disc-shaped plaster (built-in counterweight plate) is placed into the bucket cup ① to help it sink into the tanks. A long bridge was fixed at the mouth of the barrel cup ②. The bucket cup ② (built-in sealed industrial iron sand, 1 kg) was put in the bucket cup ①. Wooden strips were fixed on the upper wall of the cold and hot water sinks. When the bucket cup ① hanging on the loading rod sunk into the sinks, the long bridge of the bucket cup ② came into contact with the wooden strips, thus realizing the separation between the bucket cup ① and the bucket cup ②. In this way, the dye solution in the bucket cup ① can be subjected to the mechanical pressure generated by the separation and collision between the two barrels. 50 mg BTO, 50 mg BTO + 2.5 mg C, and 50 mg BTO + 2.5 mg C + 450 mg PVDF were added into the bucket cup ① with 50 mL dye, respectively. 1 mL of these solutions were removed to determine the concentration of dye solution after 50 times, 100 times, and 200 times temperature transformation in each group.

Then, the cooling–heating cycle test was performed. The cold-water tank was set to 20 °C, the hot water tank was set to 50 °C, the conversion time between the tanks was set to 20 s, and the residence time in the tank was set to 30 s. 50 mL of 5 mg L^{-1} solution of RhB was put into a 500 mL capacity polypropylene bucket cup ① (polypropylene, PP5, tolerance temperature of −10 °C to 120 °C). A bowl cup ③ (built-in sealed industrial iron sand, 1 kg) was put on it, which can help the bucket cup ① sink into the sink and reduce the evaporation of the solution in the bucket cup ①. The bucket cup ① was hung on the load rod and fixed it well. 50 mg BTO, 50 mg BTO + 2.5 mg C, and 50 mg BTO + 2.5 mg C + 450 mg PVDF were added into the bucket cup ① with 50 mL dye, respectively. 1 mL of these solutions were removed to determine the concentration of dye solution after 50 times, 100 times, and 200 times temperature transformation in each group.

Finally, the mechanical pressure and cooling–heating cycle test was performed. The cold-water tank was set to 20 °C, the hot-water tank was set to 50 °C. The other settings were the same as the mechanical pressure cycle test above. After the

Open Access Article. Published on 10 March 2025. Downloaded on 7/21/2025 10:40:31 PM. This article is licensed under a Creative Commons Attribution-NonCommercial 3.0 Unported Licence.

cycle of 50 times, 100 times, and 200 times, 1 mL of these solutions were taken out for the measurement of the concentration of each group solution under temperature change and mechanical pressure transformation (the specific experimental procedures are given in the videos and pictures in the ESI†).

Dental whitening experiment

The extracted premolars that we selected (with the informed consent of the donor) were healthy and without caries or defects. The teeth were immediately immersed in a 0.5% chloramine-T solution for one week after tooth extraction. Then, each tooth was washed with deionized water, soft tissues and surface soft dirt or calculus were removed, and the teeth were placed in a mixture of espresso and black tea for one week. Finally, the teeth were washed with deionized water until the washing water became clear and the teeth were dried naturally.

The stained teeth were randomly divided into the control groups, the BCPCF group, and the 30% H_2O_2 group. Each group had seven teeth. A plastic straw was cut into seven sections to wrap the teeth. These sections were coated with the separation agent. A seven-hole plaster model for tooth-supporting was prepared with the die perfusion method. The teeth of each group were placed into the seven-hole plaster model. Then, the seven-hole plaster model was put into the bucket cup ① with 50 mL deionized water. The experimental method of the mechanical pressure and cooling–heating cycle test was used to perform the dental whitening experiment. These teeth were observed after the 25 times, 50 times, 100 times, 200 times, and 400 times cycles, respectively. Among them, the teeth of the BCPCF group and the 30% H_2O_2 group were covered with the BCPCF before the mechanical pressure and cooling–heating cycle test. In addition, the teeth of the 30% H_2O_2 group were taken off the BCPCF and were placed in 30% H_2O_2 solution for 30 min before each observation.

The color values of the crowns were recorded according to the CIE Lab (Commission Internationale De L'eclairage) system. To quantitatively analyze the effect of tooth whitening, three parameters in the color space were used to characterize the color change. The value of brightness L ranged from 0 to ~100, the higher the value, the brighter the tooth surface; Δa indicated the change of color value on the red and green axis, a positive value indicated red, a negative value indicated green; Δb indicated the change of color value on the blue and yellow axis, a positive value represented yellow, and a negative value represented blue. ΔE was calculated according to formula (3) and was generally used to indicate the degree of color change. The experiments were approved by the Institutional Review Board of the School of Stomatology, Southwest Medical University (approval number: 20220809001).

$$\Delta E = \sqrt{\Delta L^2 + \Delta a^2 + \Delta b^2} \tag{3}$$

Then, the BCPCF was tested for reactive oxygen generation capacity. 50 mg thermal catalyst was placed in 50 mL deionized water and 50 ml dimethyl sulfoxide to obtain $^{\bullet}OH$ and $^{\bullet}O_2^-$ after the 25 times, 50 times, 100 times, 200 times, and 400 times of the mechanical pressure and cooling–heating cycle test. 200 μL of solution was moved out to add 20 μL of 5,5-dimethyl-1-pyrrololine *n*-oxide (DMPO) in it and was tested immediately using an electronic paramagnetic resonance instrument (Electron Paramagnetic Resonance Instrument, EPR, Brooke A 200 spectrometer).

$$q^- + O_2 \rightarrow {}^{\bullet}O_2^- \tag{4}$$

$$q^+ + H_2O \rightarrow {}^{\bullet}OH \tag{5}$$

Test of dental damage

To analyze the effect on tooth enamel after the whitening test with the BCPCF, we observed a flat area on the tooth surface of each group by SEM. Then, the teeth of each group were sliced along the cheek tongue. The Vickers microhardness meter was used to test the high buccal point, cheek point, central fossa, tongue point, and high tongue surface point of these teeth with 200 g pressure. According to the average diagonal length of the indentation, the microhardness and the indentation depth were calculated with formula (6) and formula (7), respectively.

$$HV = 1.854 \times \frac{F}{d^2} \tag{6}$$

$$h = \frac{d}{7} \tag{7}$$

Cytotoxicity test

DMEM high glucose medium with the BCPCF was immersed (6 cm^2 : 1 mL) in an atmosphere containing 5% CO_2 for 24 h, and then the extracted supernatant was centrifuged at 1000 rpm for 5 min. 100 μM H_2O_2 solution was prepared with DMEM high glucose medium. Those solutions were mixed respectively with 10% FBS and 1% penicillin–streptomycin solution. Then, they were co-cultured with human gingival fibroblasts for 1 day, 2 days, and 3 days, respectively. The live & dead animal cell viability/toxicity detection kit (calcein AM, PI) and the CCK-8 kit (CCK-8 kit) were stained for 30 min. Cell viability was calculated using formula (8) with the absorbance at 450 nm. Cell number and cell morphology were visualized by an inverted fluorescence microscope (Olympus IX73, Japan). The live cells were stained in green and the dead cells were stained in red.

$$\text{Cell viability (\%)} = \frac{A_{\text{Sample}} - A_{\text{blank}}}{A_{\text{Control}} - A_{\text{blank}}} \times 100\% \tag{8}$$

Statistical analysis

Statistical analyses were performed by one-way analysis of variance (ANOVA) and *T*-test (LSD) using SPSS 24.0 and GraphPad Prism version 10.0.2 software. A probability value (p-value) < 0.05 was considered statistically significant.

Results and discussion

Preparation and characterization of the BTO/C/PVDF composite film (BCPCF)

The BTO/C/PVDF composite film (BCPCF) was prepared by the solution casting method. The morphology of the synthesized sample was observed by using a scanning electron microscope

© 2025 The Author(s). Published by the Royal Society of Chemistry

Open Access Article. Published on 10 March 2025. Downloaded on 7/21/2025 10:40:31 PM.
This article is licensed under a Creative Commons Attribution-NonCommercial 3.0 Unported Licence.

(Fig. 2a). The graphite and the BTO were roughly evenly distributed in the PVDF material and were stably combined with it. The graphite appeared as particles with a diameter of about 20 μm (Fig. 2a1). The BTO appeared as particles with a diameter of about 0.6–1 μm (Fig. 2a2). The Fourier infrared spectrum showed that the C-F bond of PVDF molecules showed a strong absorption peak in the wavelength range of 1100–1300 cm^{-1}. This indicated that the PVDF film (PF), the BTO/PVDF composite film (BPCF), and the BCPCF were all based on the PVDF. The Ti–O bond of the BTO exhibited an absorption peak at around the 570 cm^{-1} wavelength due to the contraction vibration (Fig. 2b). This indicated the successful binding of the BTO and the PVDF in the composite film. In addition, due to the graphite doping of the BCPCF, the absorption peak wave of the Ti–O bond of the BTO was increased. The bond energy was enhanced, which might be related to the better ferroelectric performance of the BTO. The X-ray diffraction profiles represented characteristic peaks of the BTO in (100), (110), (111), (002), (200), (201), (210), (112), (211), (202), (220), (301), and (310). In particular, the five sets of double peaks of (002), (200), (201), (210), (112), (211), (202), (220), (301), and (310) can indicate the presence of a tetragonal crystalline phase of BTO, indicating that the BTO particles still have the property of spontaneous polarization in the composite film. The characteristic peaks of graphite can be seen in C (002) and C (004). The characteristic peaks of PVDF were annotated in α and β and represented the stable and polar phases of PVDF, respectively. The addition of the BTO particles increased the formation of β-phase crystallization in the PVDF, improving the piezoelectric and pyroelectric properties of the basement film, which may further improve the comprehensive performance of the BCPCF (Fig. 2c). The above results confirmed the successful synthesis of the BCPCF.

The data of the tensile and the flexural measurements showed that the tensile strength of the BCPCF was 9.0817 MPa (Fig. 2d) and the elasticity modulus was 74.1624 MPa (Fig. 2e). This indicated that the BCPCF was a flexible material with high flexibility, not easy to break.

The ferroelectric properties of BCPCF were characterized by piezoelectric responsive force microscopy (PFM). From the amplitude image in Fig. 2f, the amplitude of the composite film vibration can be estimated under the influence of the

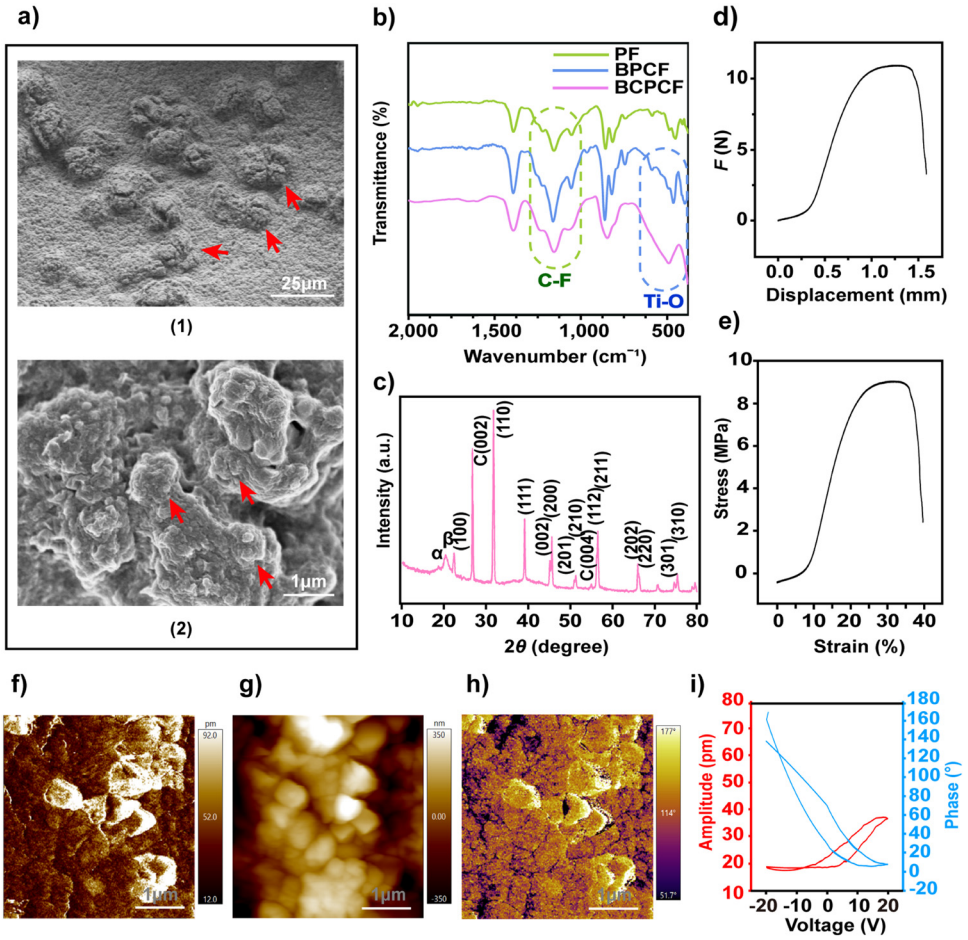

Fig. 2 The characterization of the BCPCF. (a) SEM image of the BCPCF. (1) and (2) indicate the C particles and the BTO particles, respectively. (b) FT-IR image of the PF, the BCPCF and the BPCF. (c) X-ray image of the BCPCF. (d) and (e) indicate the tensile strength and the elasticity modulus of the BCPCF respectively. (f)–(i) indicate the amplitude, the height-line, the phase, and the local piezoelectric hysteresis loop image of the BCPCF. Data are means ± SD (n = 3).

Open Access Article. Published on 10 March 2025. Downloaded on 7/21/2025 10:40:31 PM.
This article is licensed under a Creative Commons Attribution-NonCommercial 3.0 Unported Licence.

electric field. The phase diagram is shown in Fig. 2h, where the bright and dark regions of the BTO particles correspond to domains in the rightwards and leftwards directions, indicating the ferroelectric properties of the BTO particles in the composite film. The local piezoelectric hysteresis loop of BCPCF is shown in Fig. 2i, with a full change of 180° under a 20 V field. The phase switching and the amplitude loop showed a butterfly shape, implying the clear polarization of the BTO particles. According to the piezoelectric response force test results, BCPCF has piezoelectric and ferroelectric properties.

Whitening effect

According to the standard curve of the RhB concentration and OD value (Fig. 3a), when the detection wavelength was at 500 nm, the change in OD value was most significant with the increase of the RhB concentration. Based on this wavelength, the standard curve of the RhB concentration *versus* OD (Fig. 3b) was given the formula (9). In this function, R^2 = 0.996136, $P < 0.0001$, the fit of the function was very high and close to the real case. Therefore, the remaining RhB

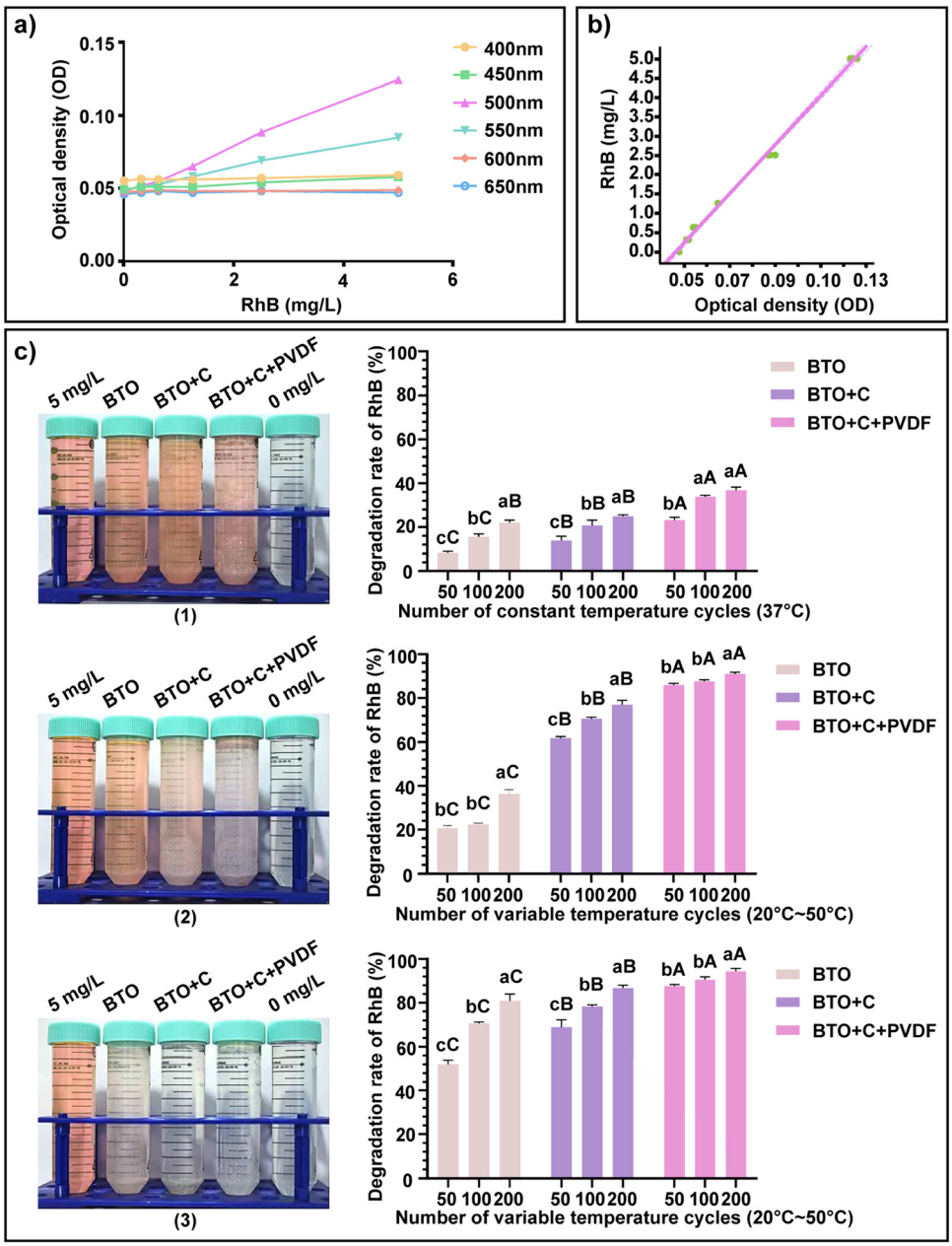

Fig. 3 Rhodamine 6G dye (RhB) degradation test. (a) OD values of PhB of standard concentration at different wavelengths. (b) The linear relationship between RhB concentration and OD value at 500 nm wavelength. (c) The powder of BTO, BTO + C, BTO + C, and BTO + C + PVDF degraded RhB (5 mg L^{-1}) during the pressure cycling (37 °C), the cooling-heating cycling (20–50 °C), and the pressure and cooling–heating cycling (20–50 °C), respectively. (1), (2) and (3) are images of each group after 200 cycles. Data are means ± SD (n = 3). Data variability is indicated by the letter notation. A, B, and C represent intergroup differences, and a, b, and c indicate within-group differences. Different letters indicate $P < 0.05$.

© 2025 The Author(s). Published by the Royal Society of Chemistry

Open Access Article. Published on 10 March 2025. Downloaded on 7/21/2025 10:40:31 PM.
This article is licensed under a Creative Commons Attribution-NonCommercial 3.0 Unported Licence.

concentration in the solution was used to calculate the degradation rate of the RhB in the subsequent experiments.

$$\text{RhB (mg L}^{-1}) = 63.6068 \times \text{OD} - 2.96511 \quad (9)$$

According to the method described in the RhB degradation test in the experimental procedure, the mechanical pressure cycle, cooling–heating cycle, and mechanical pressure and cooling–heating cycle were carried out respectively. Mechanical pressure changes were achieved by attaching a device to the cold and heat cycle meter to simulate the possible mild collision or occlusion in human oral movement. The cycle times were counted according to the one cycle of the cold and heat cycle meter, and four mechanical pressure changes can occur during one cold and heat cycle. From the results in Fig. 3c, we know that the mechanical pressure generated in this experiment was relatively weak. When the catalytic mode was changed to thermal catalysis, the abilities of the three groups of materials to degrade the dye were all improved. When the mechanical pressure and the cooling–heating cycle were conducted simultaneously, the abilities of the three groups of materials to degrade dye were further improved, which indicated that piezoelectric catalysis and thermal catalysis can occur simultaneously and that the production of ROS can be maximized. From the three groups of materials, the addition of the graphite enhanced the ferroelectricity of the BTO, so the degradation rates of the BTO + C group were significantly greater in the experiment than that of the pure BTO group. In addition, the dye degradation rates were further increased after the addition of the PVDF. This may be due to the attachment of dye to the PVDF surface.

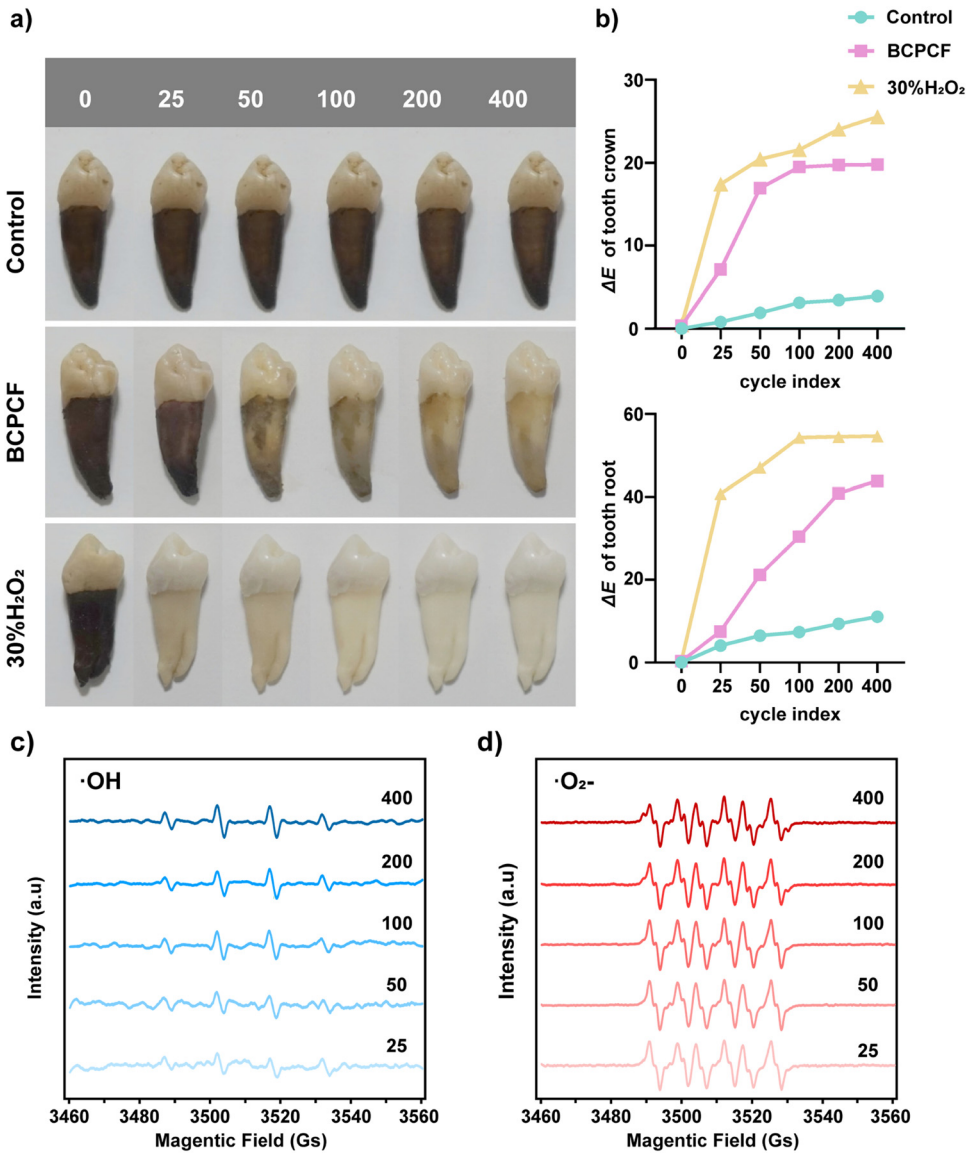

Fig. 4 Teeth-whitening. (a) Image of three tooth groups after 0, 25, 50, 100, 200, and 400 treatments. (b) The CIE Lab differences of teeth crown and teeth root after treatments of three groups. (c) and (d) Composites generated hydroxyl radical signals and superoxide anion signals under experimental conditions, respectively. Data are means ± SD (n = 3).

Open Access Article. Published on 10 March 2025. Downloaded on 7/21/2025 10:40:31 PM.
This article is licensed under a Creative Commons Attribution-NonCommercial 3.0 Unported Licence.

The tooth whitening experiment was conducted according to the mechanical pressure and cooling–heating cycle experimental method. The collected teeth were randomly divided into the control group, the BCPCF group, and the 30% H_2O_2 group. The control group only performed the mechanical pressure and cooling–heating cycle experiments. The teeth of the BCPCF group were placed with the BCPCF before the mechanical pressure and cooling–heating cycle experiments. The teeth in the 30% H_2O_2 group were immersed in a 30% H_2O_2 solution for 30 min every time, after the same experimental procedure as in the BCPCF group. The experimental time nodes were set at the 25 times, 50 times, 100 times, 200 times, and 400 times cycles. According to the results in Fig. 4a, the teeth of the BCPCF group gradually showed their original color compared with the control group. However, the teeth of the 30% H_2O_2 group gradually showed an unnatural white. According to the results in Fig. 4b, the ΔE in the crowns and roots of the BCPCF and the 30% H_2O_2 groups gradually increased over time and then flattened out. This may suggest that the whitening effect was not infinite (Scheme 1).

According to the results of electron paramagnetic resonance experiments, this material can produce a set of signals of

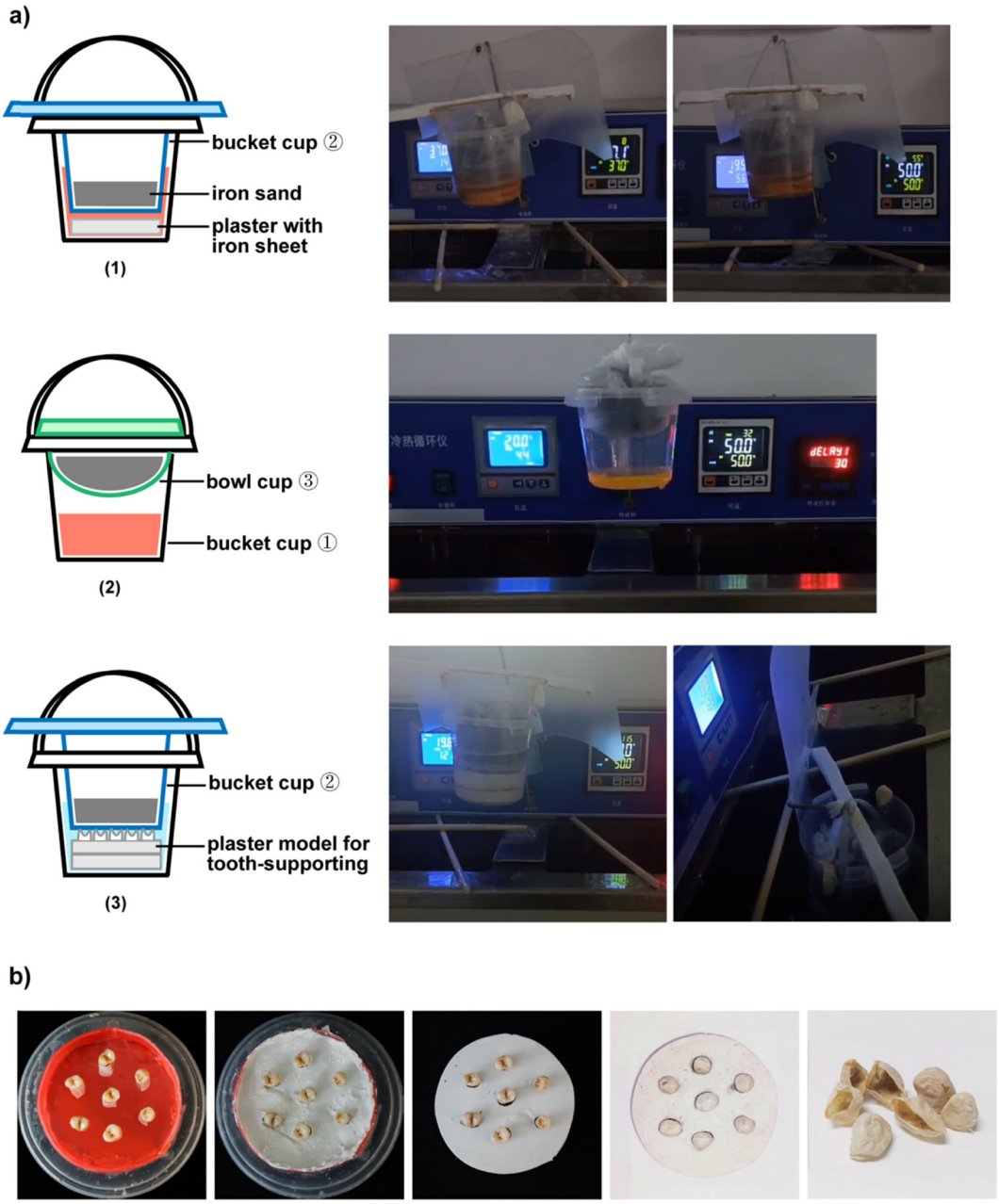

Scheme 1 ATT. 1 Equipment for whitening experiments. (a) (1) For the mechanical pressure cycle test and the mechanical pressure and cooling–heating cycle test in the RhB degradation test. (2) For the cooling–heating cycle test in the RhB degradation test. (3) For the mechanical pressure and cooling–heating cycle test in the dental whitening experiment. (b) The preparation of the plaster model for tooth-support and the image of the BCPCF.

© 2025 The Author(s). Published by the Royal Society of Chemistry

Open Access Article. Published on 10 March 2025. Downloaded on 7/21/2025 10:40:31 PM.
This article is licensed under a Creative Commons Attribution-NonCommercial 3.0 Unported Licence.

1 : 2 : 2 : 1 (Fig. 4c) and a set of signals composed of strong peaks at 1, 2, 4, and 6 and relatively weak peaks at 3 and 5 (Fig. 4d). This indicated that $^{\bullet}OH$ and $^{\bullet}O_2^-$ were successfully produced under these experimental conditions.

The degree of damage to the enamel from three sets of experimental treatments was observed by SEM. The results of Fig. 5a showed that there was no obvious demineralization on the enamel surface in the BCPCF group, and the image was not significantly different from the control group. After 30% H_2O_2 treatment, the tooth surface was demineralized and the enamel was cracked. The hardness and depth of the measured tooth surface were calculated from the mean diagonal length of the indentation. The results of Fig. 5c showed that after the treatment of the BCPCF, the hardness of the enamel surface was not significantly different from the control group, which was within the normal range (300–400). However, after the 30%

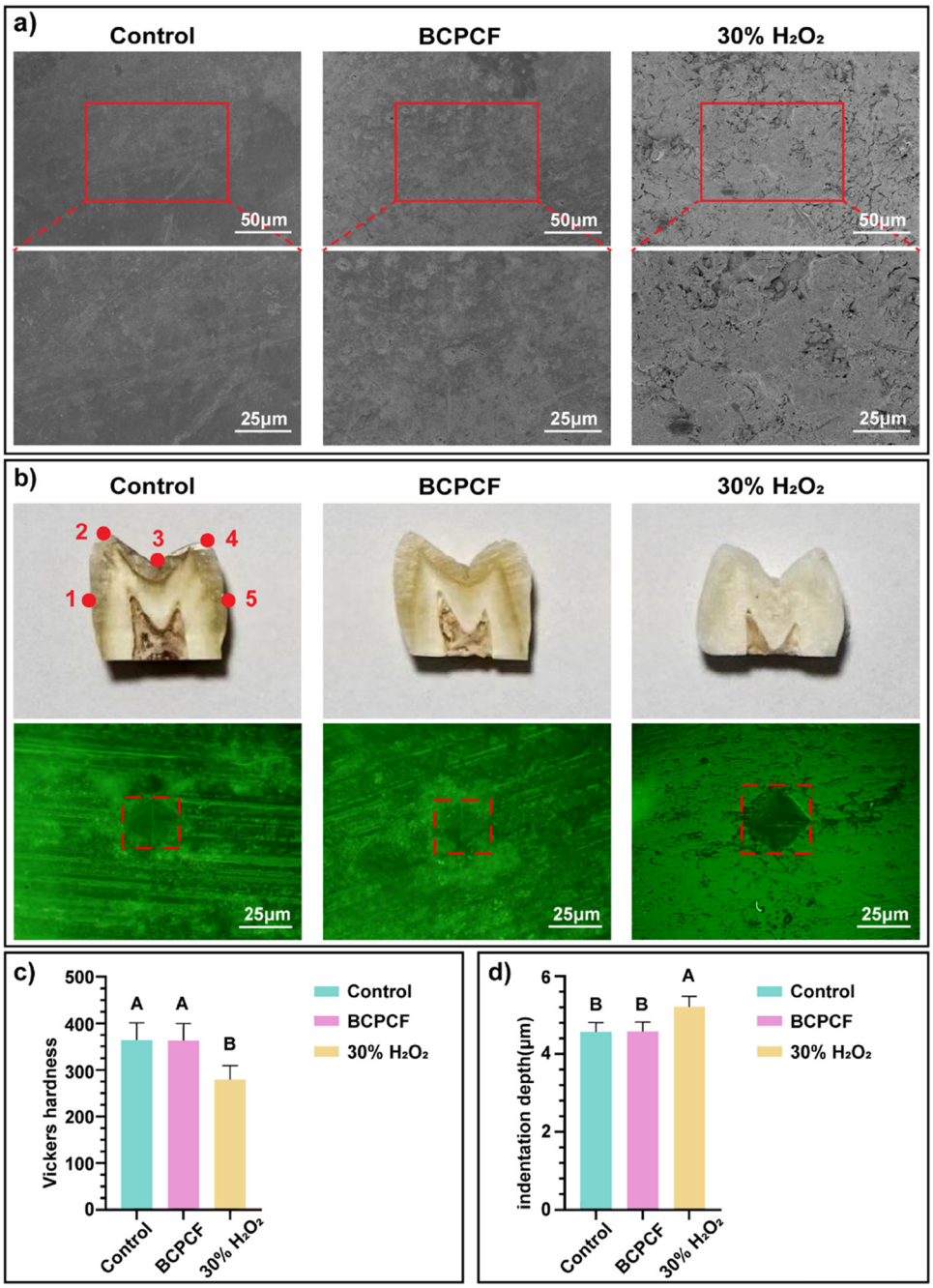

Fig. 5 Test of teeth for damage. (a) The SEM images of the tooth surface of each group after the experiment. (b) The image of the tooth sliced along the buccal-tongue direction from each group after the experiment, and the indentation image of them obtained with a Vickers hardness meter (pressure 200 g). (c) The Vickers hardness of the teeth surface of each group. (d) The depths of indentation of the teeth surface of each group. Data are means ± SD (n = 3). Data variability is indicated by the letter notation. A, B, and C represent intergroup differences. Different letters indicate $P < 0.05$.

Open Access Article. Published on 10 March 2025. Downloaded on 7/21/2025 10:40:31 PM.
This article is licensed under a Creative Commons Attribution-NonCommercial 3.0 Unported Licence.

H_2O_2 treatment, the enamel surface hardness was significantly reduced, and the indentation depth was also significantly greater than the above two groups. In conclusion, the amount of ROS produced by the BCPCF was insufficient to damage the enamel surface while ensuring good tooth-whitening effects.

Biocompatibility

Human gingival fibroblasts (HGF) were selected for the biological safety of the BCPCF. Cultured HGF cells were randomly and evenly divided into the control group, the BCPCF group and the H_2O_2 group. These groups were treated accordingly for 1 day, 2 days, and 3 days. From the results of the live and dead staining test (Fig. 6a) we observed that the living cells in the BCPCF group were long spindle-shaped, closely connected with the surrounding cells, and were stained with bright green fluorescence. The BCPCF group had only a minimal number of dead cells, which was no obvious difference from the control group. No living cells were observed in the H_2O_2 group, and all were suspended spherical dead cells with red fluorescent staining. According to the CCK-8 method (Fig. 6b), the cell viabilities of the BCPCF group were all above 80%. By the third day, the cell viability in the BCPCF group had reached 97%.

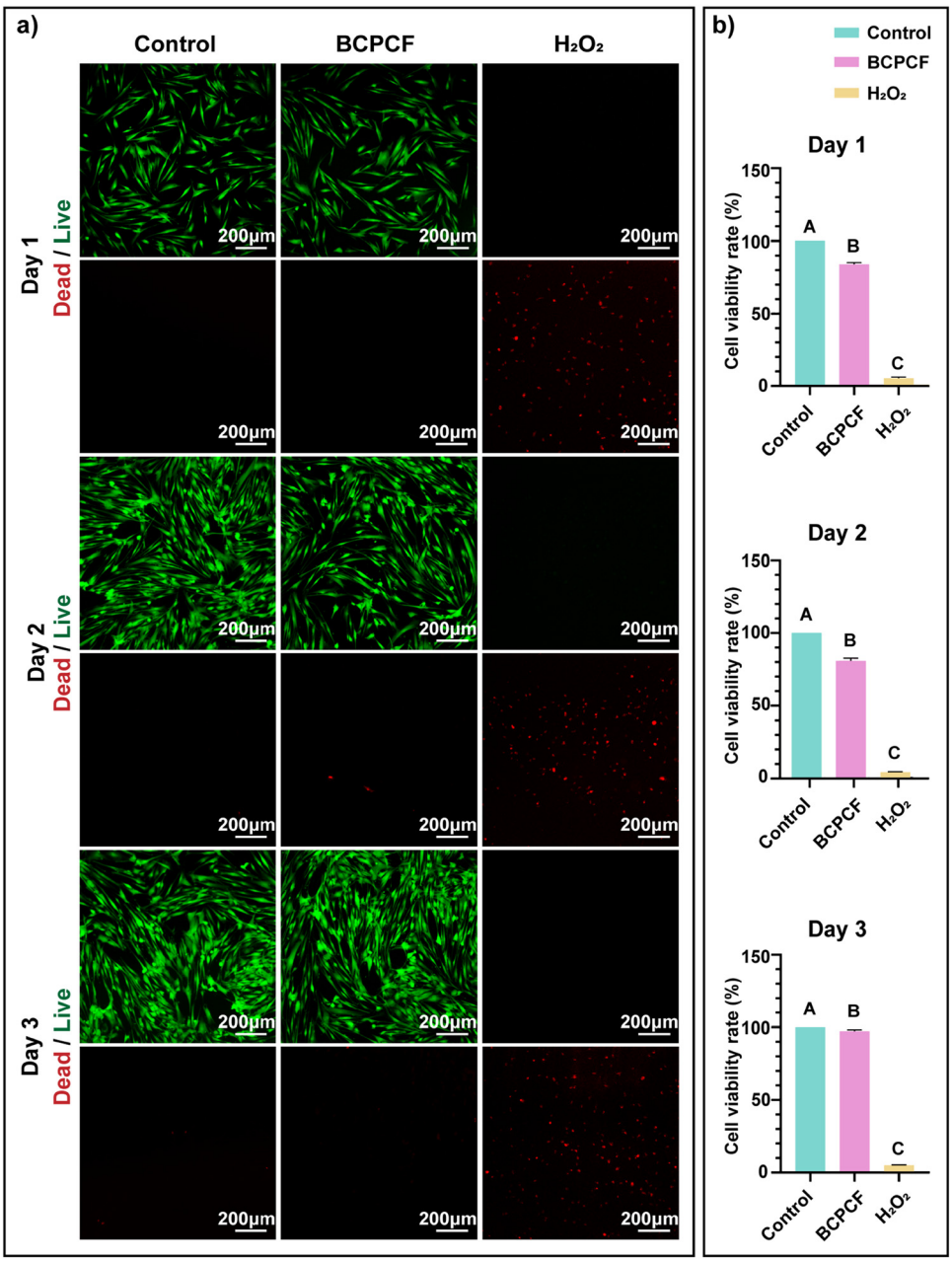

Fig. 6 Cytocompatibility assay. (a) Live/dead staining assay. Live and dead cells of HGF were stained with green and red fluorescent stains, respectively. (b) CCK8 staining assay. Cell viability of HGF for 1, 2, and 3 days. Data are means ± SD (n = 3). Data variability is indicated by the letter notation. A, B, and C represent intergroup differences. Different letters indicate $P < 0.05$.

© 2025 The Author(s). Published by the Royal Society of Chemistry

Open Access Article. Published on 10 March 2025. Downloaded on 7/21/2025 10:40:31 PM. This article is licensed under a Creative Commons Attribution-NonCommercial 3.0 Unported Licence.

However, the cell viabilities of the H_2O_2 group were all below 5%. The above results indicated that the BCPCF was not toxic to the cells and was a composite with good biocompatibility.

Conclusion

In conclusion, the BTO-based composite film can generate $^{\bullet}OH$ and $^{\bullet}O_2^-$ under mechanical pressure-cold and heat transformation, thus achieving non-destructive tooth whitening. Here, our study has many highlights. First, to our knowledge for the first time, we simulated tooth occlusion by mechanical pressure and simulated daily diet by temperature change to restore the real oral environment as much as possible. Secondly, wearing a reusable composite film effectively can reduce the workload of patients and increase the comfortable experience. Finally, the composite film can remove stains on the surface of the teeth and achieve a whitening effect without harming the teeth and periodontal tissue. However, this study still had some shortcomings. For example, although preliminary results confirmed the good biocompatibility of BCPCF, its metabolic pathways and long-term effects remain to be explored. Overall, we believe that this BCPCF is a promising strategy for future oral health care.

Author contributions

Sihan Wang: experimental design, and article writing. Yang Zhou: investigation of the piezoelectric-thermal catalytic mechanics and drawing schematic diagram. Yunan Zhang: preparation and detection of the materials. Zhongyi Yan: collecting teeth, and performing the whitening test. Liping Chen: calculation and analysis of the experimental results. Ling Guo: conceptualization, methodology, supervision, and funding acquisition. All authors discussed the results and approved the manuscript.

Data availability

The data supporting this article have been included as part of the ESI.†

Conflicts of interest

There are no conflicts to declare.

Acknowledgements

We acknowledge the support from the Luzhou Science and Technology Bureau (2024RCM239), the Sichuan Science and Technology Program (2022YFS0634 and 2024NSFSC0566), the Luzhou Key Laboratory of Oral and Maxillofacial Reconstruction and Regeneration, the Affiliated Stomatological Hospital, Southwest Medical University (Luzhou 646000, Sichuan, PR China), and the Department of Oral prosthodontics, The Affiliated Stomatological Hospital, Southwest Medical University (Luzhou 646000, Sichuan, PR China).

References

1 J. T. Newton, S. S. Subramanian, S. Westland, A. K. Gupta, W. Luo and A. Joiner, *J. Dent.*, 2021, **112**, 103771.
2 S. A. Nathoo, *J. Am. Dent. Assoc., JADA*, 1997, **128**, 6S–10S.
3 N. Lertsukprasert and K. Locharoenrat, *BMC Oral Health*, 2020, **20**, 221.
4 A. C. Branco, M. Polido, R. Colaço, C. G. Figueiredo-Pina and A. P. Serro, *Ann. Med.*, 2021, **53**, S52–S52.
5 U. Koc Vural, Z. Bagdatli, A. E. Yilmaz, F. Yalçın Çakır, E. Altundaşar and S. Gurgan, *Clin. Oral Invest.*, 2021, **25**, 5977–5985.
6 N. A. Silva, A. F. da Silva, J. L. de Sá and M. M. B. P. João, *Brazilian J. Implantology Health Sci.*, 2023, **5**, 2999–3013.
7 S. Dias, L. Casqueiro, R. Pereira, J. Silveira, A. Mata and D. Marques, *Materials*, 2023, **16**, 5552.
8 D. Wang, G. Wang, S. Murakami, Z. Fan, A. Feteira, D. Zhou, S. Sun, Q. Zhao and I. M. Reaney, *J. Adv. Dielectr.*, 2018, **08**, 1830004.
9 Y. Du, W. Sun, X. Li, C. Hao, J. Wang, Y. Fan, J. Joseph, C. Yang, Q. Gu, Y. Liu, S. Zhang and Z. Cheng, *Adv. Sci.*, 2024, **11**, 2404483.
10 D. Masekela, N. C. Hintsho-Mbita, B. Ntsendwana and N. Mabuba, *ACS Omega*, 2022, **7**, 24329–24343.
11 C. Dai, Z. Shi, Y. Xu, L. Su, X. Li, P. Deng, H. Wen, J. Wang, Q. Ye, R. P. S. Han and Q. Liu, *Adv. Healthcare Mater.*, 2025, **14**, 2401269.
12 Y. Wang, S. Wang, Y. Meng, Z. Liu, D. Li, Y. Bai, G. Yuan, Y. Wang, X. Zhang, X. Li and X. Deng, *Nat. Commun.*, 2022, **13**, 4419.
13 A. Sood, M. Desseigne, A. Dev, L. Maurizi, A. Kumar, N. Millot and S. S. Han, *Small*, 2023, **19**, 2206401.
14 X. Hu, L. Xie, Z. Xu, S. Liu, X. Tan, R. Qian, R. Zhang, M. Jiang, W. Xie and W. Tian, *ACS Appl. Mater. Interfaces*, 2021, **13**, 35315–35327.
15 Q. Li, J. Liu, Y. Xu, H. Liu, J. Zhang, Y. Wang, Y. Sun, M. Zhao, L. Liao and X. Wang, *ACS Appl. Mater. Interfaces*, 2022, **14**, 28427–28438.
16 G. Pan, H. Wang, Z. Li, J. Zheng, B. Peng, Q. Duan and M. Zhang, *Colloids Surf., B*, 2024, **243**, 114133.
17 A. A. El-Gamal, R. Mounir, E. M. Gaber and M. M. El Zayat, *Synth. Met.*, 2024, **308**, 117718.
18 R. K. Goyal, P. Tamhane and S. Tambat, *J. Mater. Sci.: Mater. Electron.*, 2021, **32**, 28468–28479.
19 X. Zhang, C. Tan, Y. Ma, F. Wang and W. Yang, *Compos. Sci. Technol.*, 2018, **162**, 180–187.
20 A. C. Patsidis, K. Kalaitzidou and G. C. Psarras, *Mater. Chem. Phys.*, 2012, **135**, 798–805.
21 S. Aodkeng, R. Rianyoi, A. Ngamjarurojana and A. Chaipanich, *Ferroelectrics*, 2018, **526**, 161–167.
22 S. Ali, H. Ali, M. Afaq, K. Mehmood, M. Uzair and W. Ahmad, *Mater. Sci. Semicond. Process.*, 2024, **181**, 108606.
23 H. Aldulaimi, G. Pircheraghi and A. Nemati, *Polym. Compos.*, 2024, **45**, 9919–9935.
24 H. Ali, M. Uzair, Y. Iqbal, M. Ali and W. Ahmad, *Mater. Sci. Eng.: B*, 2023, **296**, 116655.

© 2025 The Author(s). Published by the Royal Society of Chemistry

Open Access Article. Published on 10 March 2025. Downloaded on 7/21/2025 10:40:31 PM.
This article is licensed under a Creative Commons Attribution-NonCommercial 3.0 Unported Licence.

25 J. Liu, M. Zhang, L. Guan, C. Wang, L. Shi, Y. Jin, C. Han, J. Wang and Z. Han, *Polym. Test.*, 2021, **100**, 107236.
26 J. Lu, K. Zhang, D. Hazarika, L. Xu, J. Li, J. Wu, M. Naeem Shah, H. Jin, S. Dong, Y. Huang, Q. Zhang, Y. Wu and J. Luo, *Adv. Energy Sustainability Res.*, 2024, **5**, 2300237.
27 F. Mokhtari, S. Danti, B. Azimi, F. Hellies, E. Zanoletti, G. Albertin, L. Astolfi, R. J. Varley and J. M. Razal, *Energy Environ. Mater.*, 2025, **8**, e12807.
28 A. G. Diez, N. Pereira, R. S. Pinto, R. Gonçalves, C. M. Costa and S. Lanceros-Mendez, *J. Alloys Compd.*, 2024, **989**, 174372.
29 Y. Zhang, C. Liu, B. Jia, D. Ma, X. Tian, Y. Cui and Y. Deng, *npj Flex Electron*, 2024, **8**, 1–11.
30 X. Ren, N. Meng, L. Ventura, S. Goutianos, E. Barbieri, H. Zhang, H. Yan, M. John Reece and E. Bilotti, *J. Mater. Chem. A*, 2022, **10**, 10171–10180.
31 A. Bhiogade, K. Nagamalleswari, P. Mandal and R. V. K. Mangalam, *J. Polym. Res.*, 2023, **30**, 288.
32 O. M. Hemeda, A. Tawfik, M. M. El-Shahawy and K. A. Darwish, *Eur. Phys. J. Plus*, 2017, **132**, 333.
33 A. Ferri, S. Barrau, R. Bourez, A. Da Costa, M.-H. Chambrier, A. Marin, J. Defebvin, J. M. Lefebvre and R. Desfeux, *Compos. Sci. Technol.*, 2020, **186**, 107914.
34 S. F. Kasbi, S. H. Jafari, H. A. Khonakdar, V. Goodarzi and A. Torabi, *J. Appl. Polym. Sci.*, 2020, **137**, 49403.

© 2025 The Author(s). Published by the Royal Society of Chemistry